Journal of Magnetism and Magnetic Materials 428 (2017) 165–170

Contents lists available at ScienceDirect

Journal of Magnetism and Magnetic Materials

journal homepage: www.elsevier.com/locate/jmmm

Structure and magnetic properties of amorphous Fe-(Zr,Nb)-B melt spun alloys

J. Zamora*, I. Betancourt

Departamento de Materiales Metálicos y Cerámicos, Instituto de Investigaciones en Materiales, Universidad Nacional Autónoma de México, México D.F. 04510, Mexico

ARTICLE INFO

Keywords:
Amorphous alloys
Magnetic materials
Radial distribution function
Magnetocaloric effect
Melt-spinning

ABSTRACT

In this work, we report the structure and magnetic behavior of an amorphous $Fe_{81}Zr_5Nb_4B_{10}$ melt-spun alloy. The radial distribution function (RDF) afforded the resolution of the nearest-neighbor configuration on the basis of the atom-pair distance information, for which the positions of each peak indicated the atom-to-atom separation involved for short-range ordering. The first peaks of RDF were attributed to the distances of B-B, Fe-Fe and Zr-Nb atomic pairs, indicating a glassy structure equivalent to a distorted bcc-Fe cluster. From magnetic measurements, a magnetic moment of 0.65 Bohr magneton per Fe atom was established, together with a Curie temperature of 334 K and an initial *ac* permeability of 550 for frequencies as high as 250 kHz. In addition, the magnetocaloric effect, quantified from isothermal magnetization measurements through the magnetic entropy variation, reached a maximum of 2.0 J/kg K for a magnetic field change of 2.0 T.

1. Introduction

A considerable amount of amorphous metals (also known as "metallic glasses") have been developed since the first Au-Si alloy was obtained by rapid solidification in 1960 [1]. An important category of metallic glasses are the TM-M alloys (TM=Ni, Fe or Co and M=P, B) [2,3]. These alloys usually exhibit good glass-forming ability due to the strong chemical affinity between the TM and the metalloid species. In general, the base composition to obtain magnetic amorphous alloys of this type is $TM_{100-x}M_x$, with $10 < x < 25$ [4,5]. Amorphous alloys are commonly divided into two major groups: Fe-based and Co-based alloys. The Fe-based amorphous alloys containing around 80 at% Fe have high saturation magnetization (between 1.1 and 1.8 T, according to the metalloid content), together with large values of saturation magnetostriction λ_s (of $10x10^{-6}$ or higher) [6,7]. These alloys are also able to retain high magnetic permeability at ample frequency intervals. On the other hand, Co-based amorphous alloys containing ~60 at% Co, display nearly zero magnetostriction ($\lambda_s \sim 0$), wich makes them insensitive to mechanical stresses. These kinds of alloys are characterized by intermediate saturation magnetization values, usually within the range 0.5 to 0.8 T, alongside very high relative permeability (10^4 or more) and small coercive fields as low as (40 A/m) [8,9]. In particular, an attractive group of Fe-based metallic glasses are Fe-(Zr,Nb)-B alloys, which have been used in a wide range of applications (common-mode choke coils, pulse-transformers, power transformers, magnetic heads, sensors, electromagnetic interference devices and integrated service digital networks (ISDN), among others [10–17] due to their excellent soft magnetic behavior, characterized by ultra-low coercive field (below 80 A/m), high saturation magnetization (of up to 1.20 T), high value of relative permeability (of up to 10^5) and a wide interval of Curie temperatures (between 300 and 520 K) [9,18–20]. The presence of low H_c has been also reported for powdered amorphous materials by P. Marín *et al.* [21]. All these magnetic properties are strongly dependent on the B content.

An additional aspect of interest for the study of magnetic amorphous alloys is the description of their short-range atomic ordering, for which several models have been reported, specially for Fe-B based amorphous alloys [22–25], alongside theoretical methods such as first principles calculations for atomic structure of rapidly quenched alloys [26]. For instance, Y. Geng et al. [27] proposed the "first-neighbor" cluster model, which comprises a polyhedron of Fe atoms with a Boron atom seated at the center. Further computational studies, based on Monte Carlo equilibration and reverse-Monte Carlo simulation techniques, revealed that such B-centered prisms can become highly deformed when B contents overcome 9 at% [28]. These prisms form distinctive regions of clusters with high or low coordination. A very useful characterization tool for the experimental study of the short-range atomic ordering in amorphous alloys is the Radial Distribution Function (RDF), which describes structural changes related with local atomic arrangements, specially at short- and medium-range ordering.

* Corresponding author.
E-mail address: zamenj@iim.unam.mx (J. Zamora).

http://dx.doi.org/10.1016/j.jmmm.2016.09.121
Received 18 May 2016; Received in revised form 26 September 2016; Accepted 26 September 2016
Available online 28 September 2016
0304-8853/

RDF can be obtained from XRD data through the Fourier Integral theorem [29]:

$$RDF(r)=4\pi r^2\rho(r)dr=4\pi r^2\rho_0+(2r/\pi)\int_0^\infty S[i(S)-1]\sin(Sr)dS \quad (1)$$

where $\rho(r)$ is the number of atoms per unit volume at a distance r from a reference atom. This function $\rho(r)$ estimates the average number of atoms between r and $r+dr$. In addition, $S=4\pi\sin\theta/\lambda$ (λ is the wavelength of the radiation and θ the scattering angle) and $i(S)$ corresponds to the interference function calculated by using dispersion corrected atomic scattering for each constituent atom [3,29,30].

Complementary, the magnetocaloric effect, MCE (consisting of the adiabatic temperature change within a material subjected to the application/removal of a magnetizing field) has elicited a considerable amount of recent research across the world's materials science community, due to the possibility for developing commercial devices for magnetic refrigeration. Significant higher efficiencies are expected for this innovative technology compared with conventional cooling technologies based on gas compression/expansion cycles [31–33]. Among the variety of materials presenting MCE, Fe-rich metallic glasses were reported as capable to present an appreciable MCE, which, together with their low energy loss, higher electrical resistivity, tunable Curie transition, good mechanical behavior and corrosion resistance [34–37], makes them attractive options for magnetic refrigeration applications. The most accepted parameter for magnetocaloric characterization is the magnetic entropy variation ΔS_m, which is proportional to the temperature increase of the material caused by the application/removal of the magnetizing field. In this context, Fe-Zr-Nb-B-type amorphous alloys with different additions have been reported as having ΔS_m values within the range 0.7–2.5 J/kg K [37].

In this work, we report a systematic study on the structural and magnetic properties (including MCE) of melt spun $Fe_{81}Zr_5Nb_4B_{10}$ amorphous alloy.

2. Experimental techniques

A master ingot of the composition $Fe_{81}Zr_5Nb_4B_{10}$ was obtained by means of arc-melting of the elemental constituents in a titanium-gettered argon atmosphere. The ingot was re-melted four times to ensure chemical homogeneity. A metallic ribbon (0.9 mm width and 20-30 μm thickness) was prepared from melt-spinning process in argon atmosphere and using a wheel speed of 35 m/s. The microstructure of the as-quenched alloy was determined by means of X-ray diffraction (XRD) in a Siemens D5000 diffractometer with Co-K_α radiation, λ=1.7903 Å and step size 0.020° at 35 kV and 20 mA. The Radial Distribution Function (RDF), was calculated from X-ray diffraction pattern (Siemens D500 Mo-K_α radiation, λ=0.711 Å and step size of 0.5°). In addition, the amorphicity of the alloy was verified by means of Transmission Electronic Microscopy (TEM) in a JEOL JEM-1200 EX equipment operating at 120 kV. A thin foil of the alloy was prepared by Focused Ion Beam (FIB) JEOL JEM-9320 operated at 30 kV and 2 μA. Magnetic measurements were carried out for an as-quenched alloy sample by means of a Quantum Design Versalab system with maximum field intensity of 790 kA/m (1.0 T). Complex permeability measurements $\boldsymbol{\mu}=\mu_{re}+j\mu_{im}$ (with $j=\sqrt{-1}$) were realized in an impedance analyzer HP 4192 controlled by a PC. Our measuring system allows the determination of the complex impedance $\boldsymbol{Z}=Z_{re}+jZ_{im}$ for 94 discrete frequencies from 5-13 MHz together with voltage varying 0.1 to 1.0 V, which can be converted to longitudinal ac applied magnetic fields h_{ac} of 0.72 A/m by means of a coil with 77 turns. The conversion between complex permeability $\boldsymbol{\mu}$ and complex inductance $\boldsymbol{Z}$ formalisms is given by

$$\mu = G\left(-j\frac{Z}{\omega}\right) \quad (2)$$

Where G is an appropriate geometrical factor [38,39].

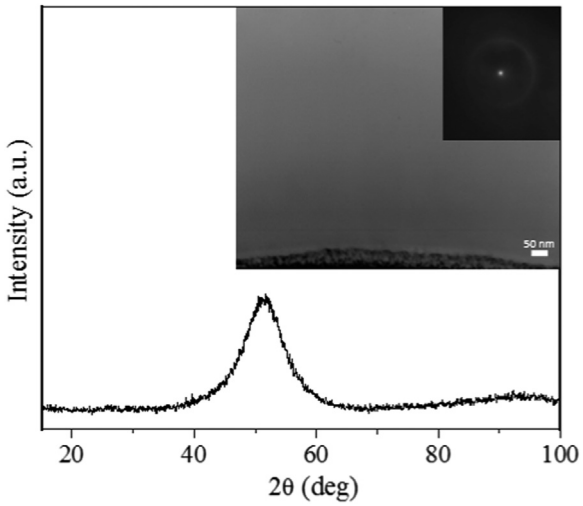

Fig. 1. XRD pattern and TEM micrograph for the melt-spun $Fe_{81}Zr_5Nb_4B_{10}$ amorphous alloy. Inset: TEM micrograph and the corresponding selected area diffraction pattern.

In addition, the magnetocaloric effect was quantified by means of the magnetic entropy variation $|\Delta S_M|$, which was calculated through the numerical integration of the Maxwell relation [32]:

$$\Delta S_M = \int_{H_0}^{H_f}\left(\frac{\partial M}{\partial T}\right)_H dH \quad (3)$$

3. Results and discussion

3.1. Structural properties

Fig. 1 shows the XRD pattern of the $Fe_{81}Zr_5Nb_4B_{10}$ melt-spun alloy, for which a single broad peak, located at 2θ ≈ 51°, corroborates the random distribution of the atomic species within the material, indicative of a fully glassy structure. The TEM micrograph (shown as inset) and the corresponding electron diffraction pattern (a single diffuse halo) for the sample also confirm an amorphous microstructure.

RDF for the $Fe_{81}Zr_5Nb_4B_{10}$ amorphous alloy is shown in Fig. 2, for which all the observed peaks were consecutively numbered.

The first peak located at 1.6 Å is attributed to B-B pair, which coincides closely with the bond length of 1.59 Å expected for B-B distance according to the boron atomic radius. Peak 2 located at 2.5 Å is attributed to the Fe-Fe pair, according to experimental reports for Fe-Fe [28,40,41]. At a distance of 3.3 Å, a shoulder-like peak suggests a Zr-Nb atomic arrangement according to the lattice parameters for the

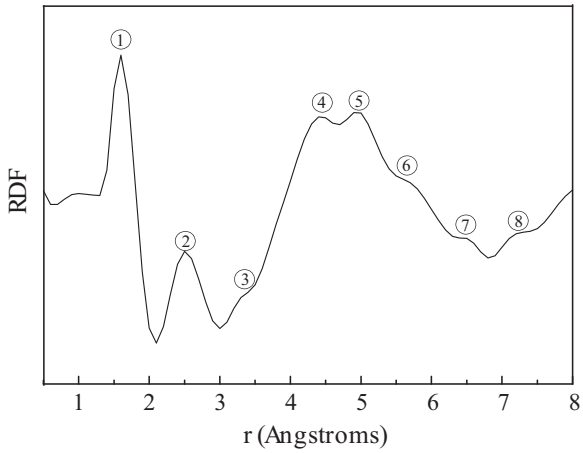

Fig. 2. Radial Distribution Function (RDF) for the amorphous $Fe_{81}Zr_5Nb_4B_{10}$ alloy.

Table 1
Atom-pair distance and peak positions for the amorphous $Fe_{81}Zr_5Nb_4B_{10}$ melt-spun alloy. A comparison of bonding lengths with other reports is included.

Peak	Pair	Distance (Å)			
		This work	[28]	[40]	[41]
1	B-B	1.6	–	–	–
2	Fe-Fe	2.5	2.5	2.5	2.54 2.53
3	Zr-Nb	3.3	–	3.5 Fe-Zr	3.36 Fe-Zr 3.35 Fe-Nb
4	Fe-B	4.4	4.4	–	–
5	Fe-Fe	4.9	4.9	4.9	–
6	Fe-B	5.7	5.7	–	–
7	Fe-Fe	6.5	6.5	6.5	–
8	Fe-Zr	7.3	–	–	–

unit cells of Zr (3.23 Å) and Nb (3.3 Å). This pair Zr-Nb replaces the Fe-Fe pair at 3.3 Å. The fourth peak located at 4.4 Å corresponds to a Fe-B pair, as suggested by computational simulations for the relative positions of Fe-B atom pairs in a cluster [28]. Peak 5 at a distance of 4.9 Å belongs to a Fe-Fe pair, according to experimental and simulation results [28,40]. Peak 6 located at 5.7 Å can be associated to a Fe-B pair, because this distance has been reported for such pair [28]. Peak 7 indicates a distance of 6.5 Å, which can be associated to a Fe-Fe pair according to the bond length reported for Fe-Fe pairs [38]. Finally, Peak (8) at distance of 7.3 Å, is close to the reported 7.2 Å value for the Fe-Zr bond [40]. This suggests that the structure is relaxed due to a greater number of B atoms within the cluster. A resume of atomic pairs, peak positions and comparison with other reports is given in Table 1.

From the atom-pair distance information provided by RDF, an atomic structure description in terms of cluster arrangements can be suggested. Each cluster comprises a polyhedral structure with central atoms. This approach affords a description of short- and medium-range atomic ordering, which has been confirmed experimentally in Fe-B amorphous alloys [40,42]. For these types of alloys, it is assumed that clusters are formed by tetrahedrons of Fe atoms, with boron occupying the central position. Alternatively, clusters with icosahedral geometry generating short-range ordering in Fe-B amorphous alloys has been studied in detail using Monte Carlo simulations [28,43]. On the basis of the atom-pair distances displayed in Table 1, we suggest for our $Fe_{81}Zr_5Nb_4B_{10}$ amorphous alloy, a short-range order similar to that of Bernal polyhedra, for which local atomic arrangement is not completely random [44]. For the cluster structure, we propose a bcc-like cell of Fe atoms surrounded by an octahedron of B atoms, such as the central position is occupied by an Fe atom, as shown in Fig. 3. As clusters are added up to the original one, some Fe atoms can be replaced by Zr-Nb pairs, causing a deformation of the bcc-like cell. A similar deformation mechanism for the disruption of the bcc symmetry (explained in terms of the inclusion of icosahedrons structures) has been described by Mackay and Bain [45] and used by other authors for describing short- and medium-range atom ordering in Fe-B amorphous alloys [28,40]. Deformations of Fe-rich regions with bcc symmetries depend on the amount of dissolved elements, such as B, Zr or Nb [28]. The assignment of Fe-Fe and Fe-B pairs for our amorphous $Fe_{81}Zr_5Nb_4B_{10}$ alloy is consistent with those proposed for similar Fe-B-based alloys [27,28,40,41].

3.2. Magnetic properties

The hysteresis loop obtained for $Fe_{81}Zr_5Nb_4B_{10}$ alloy by VSM technique is shown in Fig. 4. The magnetic behavior corresponds to a soft ferromagnetic material, since a small coercive field H_c of 5.1 kA/m is observed (inset), together with a saturation magnetization of 0.54 T.

These measurements were carried out at room temperature.

Complex permeability behavior for the amorphous $Fe_{81}Zr_5Nb_4B_{10}$ alloy is shown in Fig. 5. The spectroscopy plots $\mu_{re}(f)$ and $\mu_{im}(f)$ afford the study of the active magnetization mechanisms as a function of frequency f. For our amorphous $Fe_{81}Zr_5Nb_4B_{10}$ alloy, μ_{re} shows a plateau-like behavior for frequencies $f < 1\times10^5$ Hz. This feature is associated with reversible bulging of the magnetic domain walls pinned

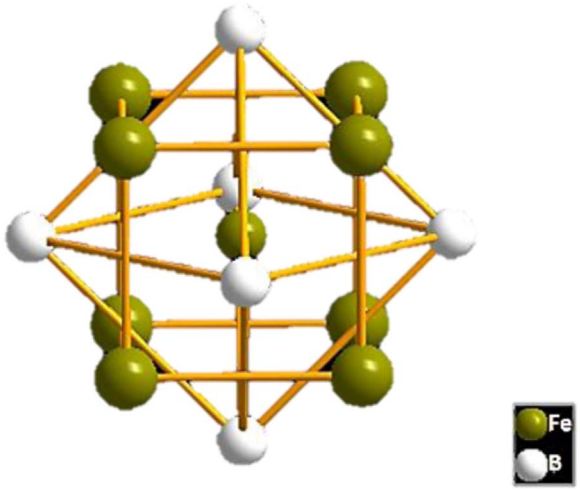

Fig. 3. Proposed polyhedron for the cluster structure of amorphous $Fe_{81}Zr_5Nb_4B_{10}$ alloy.

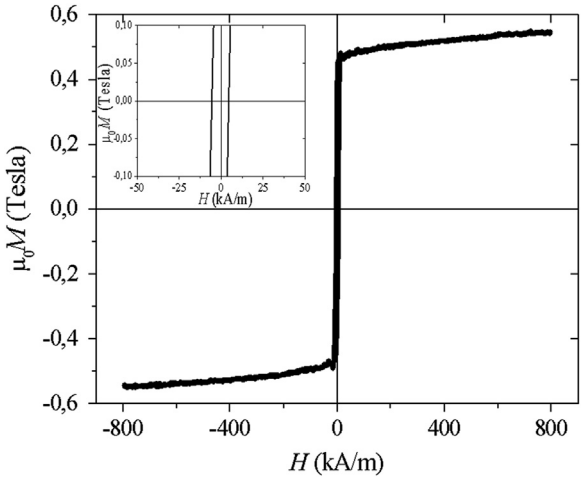

Fig. 4. M-H loop for the $Fe_{81}Zr_5Nb_4B_{10}$ melt-spun alloy.

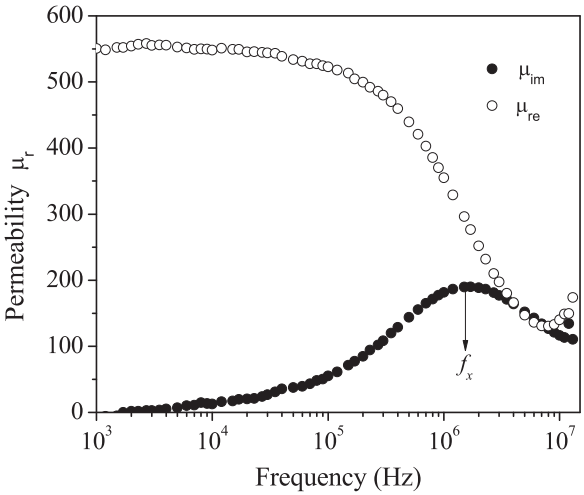

Fig. 5. Spectroscopic plots $\mu_{re}(f)$ and $\mu_{im}(f)$ for amorphous $Fe_{81}Zr_5Nb_4B_{10}$ alloy.

at the ribbon surface's defects (such as voids, surface irregularities and very surface itself), and thus, the real component of permeability μ_{re}=550 observed for this frequency interval) can be associated with the initial permeability of the material [46,47]. Further increase in f for the exciting h_{ac} causes the gradual decrease in μ_{re}, indicating the occurrence of a relaxation process for which the reversible deformation of domain walls is out of phase respect to h_{ac}. The critical frequency f_x for which reversible deformation of domain walls is no longer active as a mechanism of magnetization is known as "relaxation frequency". A noticeable high f_x=1.8 MHz was found for this alloy, which renders this alloy composition suitable for frequency-dependent applications, since an appreciable initial permeability over 500 can be sustained up to 200 kHz. To the best of our knowledge, no previous data on the spectroscopic behavior of Fe-(Zr,Nb)-B alloys have been reported.

For $f > f_x$, the active magnetization process corresponds to spin rotation, due to its smaller time constant, relative to the time constant of the reversible bulging of domain walls. On the other hand, imaginary component (μ_{im}) of the complex permeability is related to magnetic losses of the material, hysteresis and eddy currents, mainly [46,47]. The maximum value of μ_{im} coincides with f_x.

Fig. 6 displays the thermomagnetization M-T curve of the $Fe_{81}Zr_5Nb_4B_{10}$ amorphous alloy for the temperature T interval 300–380 K, at a fixed applied field of 24 kA/m. The Curie transition occurs at 334 K according to the first order derivative of the curve M-T (included as inset).

From the thermomagnetic curve, the adimensional magnetic susceptibility $\chi = M/H$ can be established with H=24 kAm. For the range $T > T_c$, the plot $1/\chi$ *vs* T can be approximated by linear fitting as shown in Fig. 7. According to the Curie-Weiss law, the effective magnetic moment μ_{eff} of the alloy can be calculated as [48].

$$\mu_{eff} = \sqrt{\frac{3k_B C}{N\mu_0}} \tag{4}$$

where k_B is the Boltzmann constant (=1.3806×10^{-23} J/K), C is the Curie constant of the material (in units of K), N is the number of atoms per unit volume (=7.8324×10^{28} atom/m^3, for $Fe_{81}Zr_5Nb_4B_{10}$ alloy), μ_0 is the magnetic permeablitiy of vacuum (=12.56×10^{-7} H/m) and μ_B is the Bohr magneton (=9.2732×10^{-24} Am^2). By considering C=0.1340 K (obtained from the linear fitting depicted in Fig. 7), the effective moment of the $Fe_{81}Zr_5Nb_4B_{10}$ alloy is μ_{eff}=0.65 μ_B per atom of Fe. This effective magnetic moment is consistent with the saturation magnetization measured in Fig. 4, as well as with the magnetic moment per atom of similar Fe-(Zr,Nb)-B amorphous alloys [49].

In addition, isothermal magnetization curves (from H=0 to H=2.0 T) are shown in Fig. 8, for which the progressive transition from the ferromagnetic to the paramagnetic state is manifested as a tendency to a linear plot as the alloy temperature approaches T_c.

From isothermal magnetization curves of Fig. 8, Arrot plots H/M vs M^2 were obteined in Fig. 9. These curves afford to identify the order of the magnetic transition, within the frame of the Landau theory of phase transitions [50]. Hence, the positive slope of the curves Arrot for $T > T_c$ indicates a second order-type transition [51].

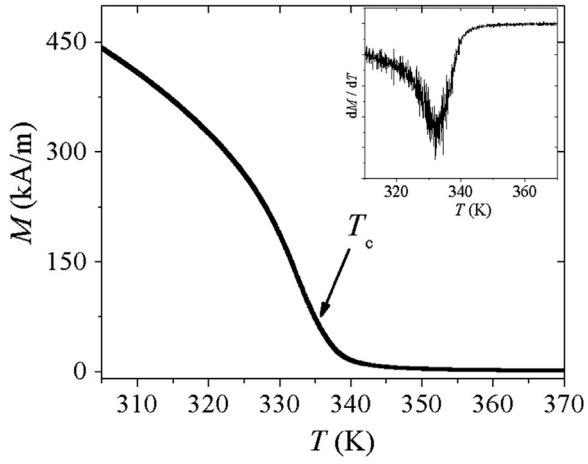

Fig. 6. Thermomagnetic M-T curve for $Fe_{81}Zr_5Nb_4B_{10}$ alloy. The inset shows temperature calculated by the first order derivative of the curve M-T.

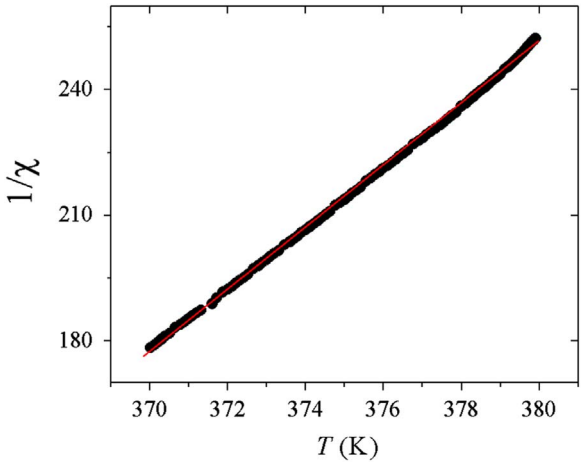

Fig. 7. Inverse magnetic susceptibility $1/\chi$ as a function of T for the $Fe_{81}Zr_5Nb_4B_{10}$ alloy for the interval $T > T_c$. The straight line (in red) corresponds to the linear fitting process, for which the resulting slope C is of 0.1340 K ± 0.5%, together with a correlation factor R^2=0.999.

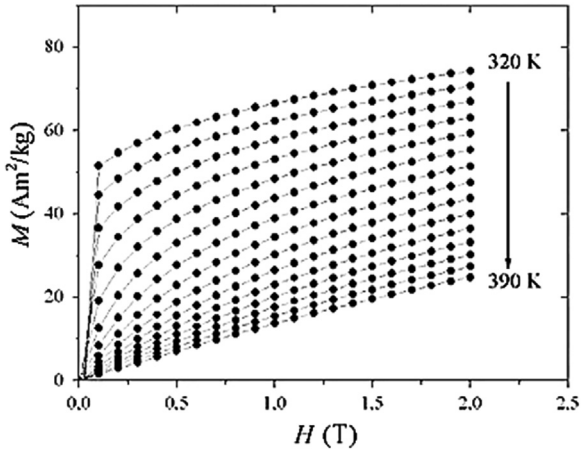

Fig. 8. Isothermal magnetization curves at variable temperature T for the $Fe_{81}Zr_5Nb_4B_{10}$ amorphous alloy.

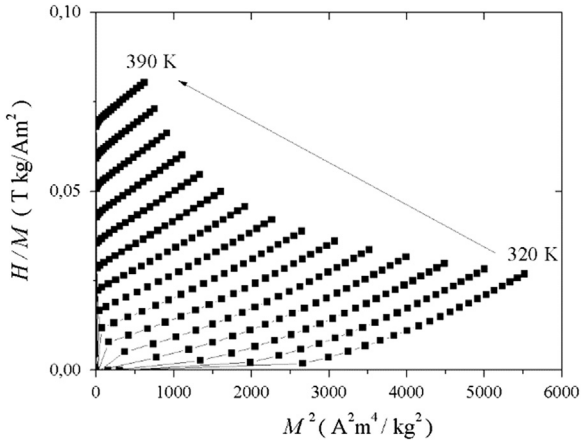

Fig. 9. Arrot plots for the $Fe_{81}Zr_5Nb_4B_{10}$ amorphous alloy. The positive slope of these curves indicates that the ferromagnetic transition is of second order.

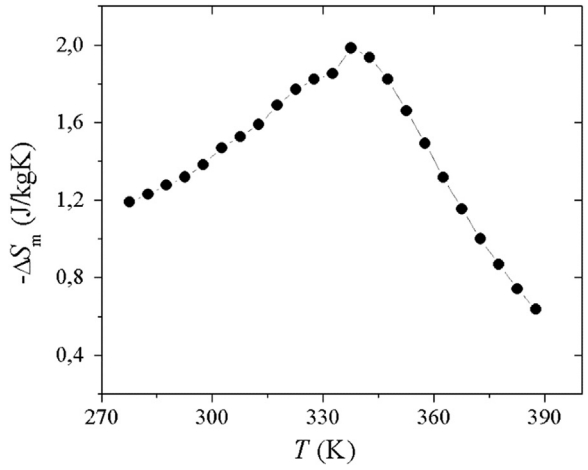

Fig. 10. Change of magnetic entropy ΔS_m for $Fe_{81}Zr_5Nb_4B_{10}$ alloy.

Magnetic entropy variation ΔS_m as a function of temperature, calculated for ΔH=2.0 T, according to Eq. (2), and data from Fig. 8, are displayed in Fig. 10 for the $Fe_{81}Zr_5Nb_4B_{10}$ amorphous alloy. A peak value of 2.0 J/kg K was observed, which results comparable with those reported for similar amorphous alloys such as Fe-Nb-B, Fe-Zr-B-Mn, Fe-Zr-B and even some nanocrystalline alloys such as Nanoperm, whose ΔS_m varies between 0.7 and of 2.5 J/kg K [32,37,52].

4. Conclusions

Data from the Radial Distribution Function of $Fe_{81}Zr_5Nb_4B_{10}$ amorphous alloy allowed the description of the atomic short-range ordering in terms of an octahedron of B atoms surrounding a distorted bcc-Fe cell. Concerning magnetic properties, a soft magnetic response was found for this type of alloys, characterized by an effective magnetic moment of 0.65 μ_B per atom of Fe and an *ac* magnetization mechanism dominated by reversible bulging of domain walls up to a relaxation frequency of 1.8 MHz. In addtion, the magnetocaloric effect, quantified by means of the magnetic entropy variation, reached a maximum of 2.0 J/kg K.

Acknowledgment

Authors are grateful with Adriana Tejeda, Carlos Flores and Gabriel Lara from IIM-UNAM, Mexico and with Victor Hugo Lara from UAM, Mexico, for their helpful technical assistance, as well as with Prof. Pedro Bosch, IIM-UNAM, for his valuable discussions of results. Authors also acknowledge the support of Dr. Jose T. Elizalde, from UACJ, Mexico, for the use of their equipment for magnetic measurements.

References

[1] W. Klement, R.H. Willens, P. Duwez, Structure in solidified gold-silicon alloys, Nature 187 (1960) 869–870.
[2] A. Inoue, Bulk amorphous Alloys; Practical Characteristics and Applications, First edition, Trans Tech Publications LTD, Vol. 6 of Materials Science Foundations, 1999.
[3] F. Luborsky, Ferromagnetic materialsFirst edition, in: E.P. Wohlfarth (Ed.), Handbook of Magnetic Materials vol. 1 (1980), 1980 North-Holland, Amsterdam.
[4] C.D. Graham Jr, T. Egami, Magnetic properties of amorphous alloys, Ann. Rev. Mater. Sci 8 (1978) 423–457.
[5] H. Kronmuller, S. Parkin, Handbook of Advanced Magnetic Materials, Vol. 4: Novel Materials, First edition Vol. 4, Wiley, New York, 2007.
[6] H. Warlimont, R. Boll, Applications of amorphous soft magnetic materials, J. Magn. Magn. Mater. 26 (1982) 97–105.
[7] A. Makino, A. Inoue, T. Hatanai, T. Bitoh, Improved soft magnetic properties and nanocristallyne Fe-M-B-Cu (M=Zr, Nb) alloys with high saturation magnetic flux density and Zero-magnetostriction, Mater. Sci. Forum. 235 (1997) 723–728.
[8] R.C. O' Handley, Physics of ferromagnetism amorphous alloys, J. Appl. Phys. 62 (1987) R15–R59.
[9] A. Inoue, T. Zhang, A. Takeuchi, Bulk amorphous alloys with high mechanical strength and good soft magnetic properties in Fe-TM-B (TM=IV-VIII group transition metal) system, Appl. Phys. Lett. 71 (1997) 464–466.
[10] N. Nishiyama, K. Amiya, A. Inoue, Bulk metallic glasses for industrial products. New structural and functional applications, in: R. Busch, T.C. Hufnagel (eds.), Simposium Proceedings of Amorphous and Nanocrystalline Metals, 2004
[11] N. Nishiyama, K. Amiya, A. Inoue, Bulk metallic glasses for industrial products: New structural and functional applications, in: J. Eckert, A. Inoue, W. L. Johnson, A. R. Yavari, Warrendale, (eds.), Symposium Proceedings of Amorphous and nanocrystalline metals, Materials Research Society, PA, vol. 806, 2004, pp. 387–392.
[12] S. Yoshida, T. Mizushima, T. Hatanai, A. Inoue, Preparation of new amorphous powders cores using Fe-based glassy alloy, IEEE Trans. Magn. 36 (2000) 3424–3429.
[13] A. Makino, T. Hatanai, A. Inoue, T. Masumoto, Nanocrystalline soft magnetic Fe-M-B (M=Zr, Hf, Nb) alloys and their applications, Mater. Sci. Eng. A 226–228 (1997) 594–602.
[14] W. Lu, L. Yang, B. Yan, B. Lu, W. Huang, Bulk amorphous and nanocrystalline $Fe_{86}Zr_{5.5}$ $Nb_{5.5}B_3$ alloy by rapid consolidation at super-high pressure, J. Magn. Magn. Mater. 292 (2005) 299–303.
[15] A. Makino, K. Suzuki, A. Inoue, Y. Hirotsu, T. Masumoto, Magnetic properties and microstucture of nanocrystalline bcc Fe-M-B (M=Zr, Hf, Nb) alloys, J. Magn. Magn. Mater. 133 (1994) 329–333.
[16] Z. Hua, Y.M. Sun, W.Q. Yu, M.B. Wei, Crystallization progress and magnetic property of Fe-Zr(Nb)-B amorphous-nanocrystalline alloy, Int. J. Mod. Phys. B 26 (2012) 1250088.
[17] A. Makino, T. Bitoh, A. Kojima, A. Inoue, T. Matsumoto, Low core losses of nanocrystalline Fe-Zr-Nb-B soft magnetic alloys with high magnetic flux density, Mater. Sci. Eng. A 304–306 (2001) 1083–1086.
[18] A. Inoue, Stabilization of metallic supercooled liquid and bulk amorphous alloys, Acta Mater. 48 (2000) 279–306.
[19] B. Yao, L. Si, H. Tan, Y. Zhang, Y. Li, Effects of high boron content on crystallization, forming ability and magnetic properties of amorphous $Fe_{91-x}Zr_5B_xNb_4$ alloy, J. Non-Cryst. Solids 332 (2003) 43–52.
[20] B. Yao, Y. Zhang, L. Si, H. Tan, Y. Li, Boron content dependence of crystalline, glass forming ability and magnetic properties in amorphous Fe-Zr-B-Nb alloys, J. Alloy Compd. 370 (2004) 1–7.
[21] P. Marín, A.M. Aragón, A. García Escorial, M. Lieblich, P. Crespo, A. Hernando, Coercivity and its thermal dependence in microsized magnetic particles: Influence of grain boundaries, J. Appl. Phys. 113 (2013) 043909.
[22] D.B. Miracle, A structural model for metallic glasses, Nat. Mater. 3 (2004) 697–702.
[23] O.N. Senkov, D.B. Miracle, Effect of the atomic size distribution on glass forming ability of amorphous metallic alloys, Mater. Res. Bull. 36 (2001) 2183–2198.
[24] P.H. Gaskell, A new structural model for amorphous transition metal silicides, borides, phosphides and carbides, J. Non-Cryst. Solids 32 (1979) 207–224.
[25] H. Hermann, N. Mattern, Analytic approach to the structure of amorphous iron-boron alloys, J. Phys. F: Met. Phys. 16 (1986) 131–140.
[26] A. García-Escorial, P. Crespo, A. Hernando, M. Lieblich, P. Marín, V. Velasco, F. Ynduráin, Magnetism microstructure and first principles calculations of atomized and annealed Ni_3Al, J. Alloy. Compd. 615 (2014) S645–S647.
[27] Y. Geng, Y. Wang, J. Qiang, G. Zhang, C. Dong, P. Häussller, Composition formulas of Fe-B binary amorphous alloys, J. Non-Cryst. Solids 432 (2016) 453–458.
[28] M. Aykol, A.O. Mekhrabov, M.V. Akdeniz, Nano-scale phase sepation in amorphous Fe-B alloys: atomic and cluster ordering, Act. Mater 49 (2001) 4069–4077.
[29] H.P. Klug, L.E. Alexander, X-Ray Diffraction Procedures for Polycrystalline and Amorphous Materials, second edition, Wiley-Interscience publication, 1974.
[30] M. Taylor, A quasi-crystalline model for interpretation of radial distribution functions: theory and experimental confirmation, J. Appl. Cryst. 12 (1979) 442–449.
[31] E. Warburg, Magnetische Untersuchungen über einige Wirkungen der Koerzitivkraft, Ann. Phys. 13 (1881) 141–164.
[32] A.M. Tishin, Y.E. Spichkin, The Magnetocaloric Effect and its Applications, Institute of Physics publishing, Bristol-Philadelphia, 2003.
[33] P. Debye, Einige Bemerkungen zur Magnetisierung bei tiefer Temperatur, Ann. Phys. 81 (1926) 1154.
[34] V. Franco, J.S. Blazquez, C.F. Conde, A. Conde, A. Finemet-type, alloy as a low-cost candidate for high-temperature magnetic refrigeration, Appl. Phys. Lett. 88 (1996) 042505.
[35] F. Johnson, R.D. Shull, Amorphous-FeCoCrZrB ferromagnets for use as high-temperature magnetic refrigerants, J. Appl. Phys. 99 (2006) 08K909.
[36] D. Mishra, M. Gurram, A. Reddy, A. Perumal, P. Saravanan, A. Srinivasan, Enhanced soft magnetic properties and magnetocaloric effect in B substituted amorphous Fe-Zr alloy ribbons, Mater. Sci. Eng. B 175 (2010) 253–260.
[37] V. Franco, J.S. Blázquez, B. Ingale, A. Conde, The magnecaloric effect and magnetic refrigeration near room temperature: materials and models, Annu. Rev. Mater. Res. 42 (2012) 305–342.
[38] I. Betancourt, Magnetization dynamics of amorphous ribbons and wires studied by inductance spectroscopy, Materials 4 (2011) 37–54.
[39] E. Amano, R. Valenzuela, J.T.S. Irvine, Domain wall relaxation in amorphous ribbons, J. Appl. Phys. 67 (1990) 5589–5591.
[40] T. Ohkubo, H. Kai, A. Makino, Y. Hirotsu, Structural change of amorphous $Fe_{90}Zr_7B_3$ alloy in the primary crystallization process studied by modern electron microscope technique, Mater. Sci. Eng. A 312 (2001) 274–283.
[41] E. Matsubara, S. Sato, M. Imafuku, T. Nakamura, H. Koshiba, A. Inoue, Y. Waseda, Structural study of Amorphous $Fe_{70}M_{10}B_{20}$ (M=Zr, Nb and Cr) alloys by X-ray

diffraction, Mater. Sci. Eng. A 312 (2001) 136–144.
[42] R. Hasegawa, R. Ray, Iron-boron metallic glasses, J. Appl. Phys. 49 (1978) 4174.
[43] C.M. Lee, K.W. Park, B.J. Lee, Y. Shibutani, J.C. Lee, Structural disordering of amorphous alloys: a molecular dynamics analysis, Scr. Mater. 61 (2009) 911–914.
[44] R.C. O'Handley, Modern Magnetic Materials: Principles and Applications, John Wiley & Sons, 1999.
[45] M. Torres, G. Pastor, I. Jimenez, J. Fayos, Geometric models for continuous transitions from quasicrystals to crystals, J. Philos. Mag. Lett. 59 (1989) 181.
[46] R. Valenzuela, Giant Magnetoimpedance and inductance spectroscopy, J. Alloy. Compd. 369 (2004) 40–42.
[47] R. Valenzuela, The Frequency Response of Magnetic Materials, Magnetic Materials: Current Topics in Amorphous Wires, Hard Magnetic Alloys Ceramics, Characterization and Modeling, in: I. Betancourt (ed.), Researcher SignPost Kerala, India, 2007, pp. 1.
[48] D. Culity, Introduction to Magnetic Materials, Second edition, Wiley, 1999.
[49] J.M. Barandiaran, P. Gorria, J.C. Gomez Sal, L.F. Barquin, S.N. Kaul, Influence of boron on the magnetic and transport properties of FeZr amorphous and nano-crystalline alloys, IEEE Trans. Magn. 30 (1994) 4776–4778.
[50] A.P. Guimaraes, Magnetism and Magnetic Resonance in Solids, first edition, Wiley -Interscience Publication, 1998.
[51] S.K. Banerjee, On generalised approach to first and second order magnetic transitions, Phys. Lett. 12 (1964) 16–17.
[52] V. Franco, J.S. Blázquez, A. Conde, Influence of Ge addition on the magnetocaloric effect of a Co-containing nanoperm-type alloy, J. Appl. Phys. 103 (2008) 07B316.